Zygote **22** (November), pp. 446–454. © Cambridge University Press 2013
doi:10.1017/S0967199413000026 First Published Online 7 March 2013

Digital holographic microscopy for the evaluation of human sperm structure

G. Coppola[1], *G. Di Caprio*[3], *M. Wilding*[2], *P. Ferraro*[4], *G. Esposito*[2], *L. Di Matteo*[2], *R. Dale*[2], *G. Coppola*[3] *and B. Dale*[2]

Centro Fecondazione Assistita (CFA-Italia), Naples; Istituto per la Microelettronica e i Microsistemi, del Consiglio Nazionale delle Ricerche, Sezione di Napoli, Naples; and Istituto Nazionale di Ottica, del Consiglio Nazionale delle Ricerche, Sezione di Napoli, Pozzuoli, Italy

Date submitted: 20.10.2011. Date accepted: 28.10.2012

Summary

The morphology of the sperm head has often been correlated with the outcome of *in vitro* fertilization, and has been shown to be the sole parameter in semen of value in predicting the success of intracytoplasmic sperm injection and intracytoplasmic morphologically selected sperm injection.

In this paper, we have studied whether digital holographic microscopy (DHM) may be useful to obtain quantitative data on human sperm head structure and compared this technique with high-power digitally enhanced Nomarski optics. The main advantage of digital holography is that high-resolution three-dimensional quantitative sample imaging may be automatically produced by numerical refocusing of a two-dimensional image at different object planes without any mechanical scanning. We show that DHM generates useful information on the dimensions and structure of human sperm, not revealed by conventional phase-contrast microscopy, in particular the volume of vacuoles, and suggest its use as an additional prognostic tool in assisted reproduction technology.

Keywords: Digitally enhanced Nomarski microscopy, Digital holographic microscopy, Human sperm structure, Male infertility, Vacuoles

Introduction

Following the advent of human *in vitro* fertilization (Steptoe & Edwards, 1978), much attention has been given to identifying first embryo morphology and, later, oocyte morphology as prognostic tools (Elder & Dale, 2011); less attention has been given to sperm morphology. The spermatozoon delivers the haploid male genome to the oocyte, introduces the centrosome and triggers the oocyte egg into activity.

[1]All correspondence to: G. Coppola. Centro Fecondazione Assistita (CFA-Italia), Via Manzoni 15, 80123 Naples, Italy. Tel: +39 081641689. Fax: +39 0815479251. e-mail: gcoppola@cfa-italia.com
[2]Centro Fecondazione Assistita (CFA-Italia), Via Manzoni 15, 80123 Naples, Italy.
[3]Istituto per la Microelettronica e i Microsistemi, del Consiglio Nazionale delle Ricerche, Sezione di Napoli, Via P. Castellino, 111, 80131 Naples, Italy.
[4]Istituto Nazionale di Ottica, del Consiglio Nazionale delle Ricerche, Sezione di Napoli, c/o Comprensorio Olivetti, Via Campi Flegrei 34 - 80078 Pozzuoli, Italy.

The sperm head may be considered in three parts: (1) the nucleus with a haploid set of chromosomes, in which deoxyribonucleic acid (DNA) is packaged into a volume that is typically less than 10% of the volume of a somatic cell nucleus (Dadoune, 2003; Elder & Dale, 2011); (2) the acrosome, a large Golgi-derived secretory vesicle on the proximal hemisphere of the head that contains an array of hydrolytic enzymes used for digesting the zona pellucida during penetration (Gerton, 2002; Yoshinaga & Toshimori, 2003); and (3) the perinuclear theca, a rigid capsule composed of disulphide bond stabilized structural proteins amalgamated with various other protein molecules (Oko, 1995).

Human spermatozoa exhibit a wide range of shapes. Several studies have indicated that sperm morphology best predicts the outcome of natural fertilization (Kruger *et al.*, 1988; Bartoov *et al.*, 1999), intra-uterine insemination (Berkovitz *et al.*, 1999), conventional *in vitro* fertilization (IVF) (Kruger *et al.*, 1988; Mashiach *et al.*, 1992) and intracytoplasmic sperm injection (ICSI) (Palermo *et al.*, 1992; Bartoov *et al.*, 2002),

https://doi.org/10.1017/S0967199413000026 Published online by Cambridge University Press

and several techniques have been described that provide valuable information on the morphology and pathological features of spermatozoa. In a classical clinical evaluation, human sperm are fixed, stained and analysed by optical microscopy. Recently, several novel techniques have been developed for the identification of more detailed features of the cells. Differential interference contrast microscopy, scanning near-field optical microscopy, electrostatic force microscopy, atomic force microscopy and scanning thermal microscopy (Akaki *et al.*, 2002; Bartoov *et al.*, 2002; Rothery *et al.*, 2003). Most of these techniques involve biochemical processing that requires specific equipment and may also alter the vitality of the sperm analysed.

The sperm cell is almost transparent in conventional bright field microscopy, as its optical proprieties differ slightly from the surrounding liquid, generating little contrast. However, a light beam that passes through a spermatozoon undergoes a phase change, in comparison with the surrounding medium, the amplitude of which depends on the light source, the thickness and the integral refractive index of the object itself. A qualitative visualization of this phase contrast may be obtained by contrast interference microscopy (phase contrast or Nomarski/Zernicke interferential contrast microscopy). Recently, efforts have been renewed to improve differential interferometric contrast methods in order to provide quantitative information in microscopy (Bon *et al.*, 2009; Kou *et al.*, 2010). On the other hand, over the last few years, digital holography in microscopy has been established as a valid non-invasive, quantitative, label-free, high-resolution, phase-contrast imaging technique. Furthermore, this technique has been applied successfully to image a variety of cell types (Carl *et al.*, 2004; Marquet *et al.*, 2005; Charrière *et al.*, 2006; Kemper *et al.*, 2006; Di Caprio *et al.*, 2010) to obtain additional information about their structure. In a recent preliminary study in human spermatozoa using digital holographic microscopy (DHM), a statistically significant difference in phase shift was observed when comparing normal sperm with oligoasthenozoospermic sperm (Crha *et al.*, 2011), however the authors did not measure standard morphological parameters using this technique, nor investigate the characteristics of sperm with nuclear vacuoles. One of the main advantages of DHM is that high-resolution three dimensional (3-D) quantitative sample imaging can be automatically produced by numerical refocusing of a two dimensional (2-D) image at different object planes without any mechanical scanning (Dubois *et al.*, 1999; Ferraro *et al.*, 2005). Moreover, using a single acquired image it is possible both to reduce the size of the mass storage devices required for image saving and to achieve a fast image transfer.

In this study, we have compared semi-automated digitally enhanced Nomarski microscopy (DESA) with DHM to study morphometrical, morphological and volumetrical measurements in normal and vacuolated human spermatozoa.

Materials and methods

Specimen collection and analytical procedures

Ejaculates were collected by masturbation from 15 males scheduled to undergo IVF at the Centro Fecondazione Assistita (CFA), Naples. After liquefaction, 0.5–1.0 ml of each specimen was processed using a double-density-gradient centrifugation method (Percoll, Sydney IVF). The final pellets were resuspended in Ham's F-10 (Gibco) and used to prepare slides for DESA. Briefly, a semen aliquot that contained 2×10^6 spermatozoa was washed twice by centrifugation with phosphate-buffered saline (PBS). Then the pellet was suspended in 100 μl of 2% formaldehyde in PBS and fixed for 10 min at room temperature. A 10-μl aliquot was then spotted onto a clean microscope slide, allowed to air dry and mounted with PBS:glycerol (1:1) (v/v).

In order to compare the same cells by both DESA and DHM, a grid of 20×20 circles (with a radius of 100 μm) was placed over the microscope. This grid was made by a photolithographic process that allows the transfer of the shape of the grid from a mask to a photo-sensitive polymer. At the end of this process, the whole surface of the slide was covered with a 1 μm-thick photo-sensitive material except the circles. A 10-μl aliquot was than spotted on the grid and finally a cover slide was placed to seal all. Only cells that fell in the circles of the grid were analysed (Fig. 1).

Slides were first examined under immersion oil using an inverted microscope (TI-DH; Nikon Instruments Italia) equipped with Nomarski optics enhanced by digital imaging to achieve a magnification of up to ×1500. The images were captured by a colour video camera for high-quality image production and analysed using image processing software (NIS-Element Documentation, Nikon).

Principles of DHM

In holography, an object is illuminated by a collimated, monochromatic, coherent light with wavelength λ. The object scatters the incoming light forming a complex wavefield (the object beam):

$$O(x, y) = |O(x, y)| e^{j\varphi(x,y)} \quad (1)$$

where |O| is the amplitude and φ the phase, x and y denote the Cartesian coordinates in the plane where the wavefield is recorded (hologram plane). The phase

https://doi.org/10.1017/S0967199413000026 Published online by Cambridge University Press

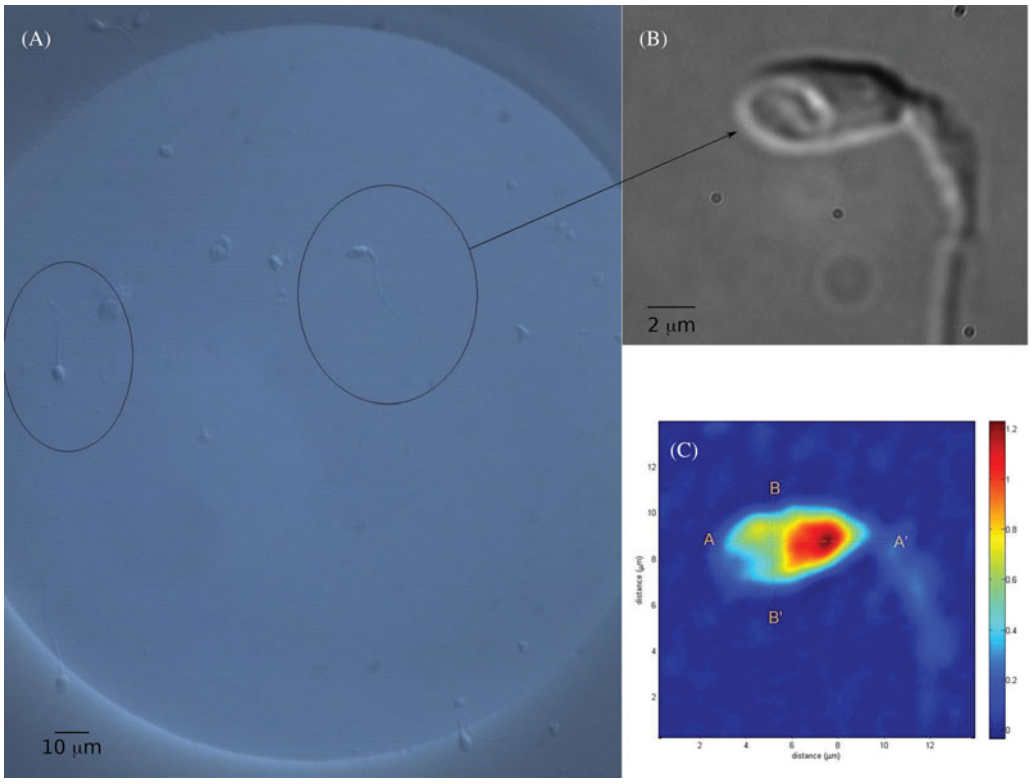


Figure 1 (*A*) A circle of a grid of 20×20 circles (with a radius of $100\,\mu m$) placed over microscope slide. (*B*) Differential interference contrast micrograph of a sperm head. (*C*) Pseudocolour plot of the same spermatozoon.

$\varphi(x,y)$ incorporates information about the topographic profile of the object under investigation because it is related to the optical path difference (OPD), which depends on the refractive index and height both of the biological sample and of the material containing the object itself:

$$\varphi(x, y) = \frac{2\pi}{\lambda} \cdot \mathrm{OPD} \tag{2}$$

where a transmission configuration has been considered. The purpose of holography is to capture the complete wavefront, and in particular the phase φ to obtain quantitative information about the topographic profile of the object (Cuche *et al.*, 1999). As all light sensitive sensors respond to intensity only, the phase is encoded in the intensity fringe pattern adding another coherent background wave $R(x,y) = |R(x,y)|e^{j\varphi(x,y)}$, called the reference beam. This beam and the object beam interfere at the surface of the recording device. The hologram is proportional to the intensity of this interference pattern. In digital holography the hologram is acquired by a charge coupled device (CCD) or a complementary metal-oxide semiconductor (CMOS) camera array, i.e. a 2-D rectangular raster of $M \times N$ pixels, with pixel pitches Δx and Δy in the two directions.

Image reconstruction

The image reconstruction procedure allows the retrieval of a discrete version of the complex optical wavefront present on the surface of the object under test. This optical wavefront is obtained by a numerical back propagation of spatially filtered product between the acquired hologram and a numerical replica of the reference beam (Cuche *et al.*, 1999; Coppola *et al.*, 2004; Ferraro *et al.*, 2004). Thus, the reconstruction procedure allows the simultaneous determination of both the intensity and, especially, the phase distribution $\varphi(m,n)$ of the optical wavefront of the specimen. Where $\phi(m,n)$ is the discretized version of the phase distribution $\varphi(x,y)$ and m,n are positive integer numbers that identify the m-th row and n-th column of the pixels matrix of the CCD (CMOS) camera. By inverting Equation (2) and considering a homogeneous material with refractive index nc, from the reconstructed phase distribution, the thickness distribution s(m,n) of the object under investigation can be obtained as follows:

$$\mathrm{OPD}_{m,n} = \frac{\lambda}{2\pi}\varphi(m, n) = \frac{\lambda}{2\pi} \arctan \frac{\mathrm{Im}[Qm, n]}{\mathrm{Re}[Qm, n]} \tag{3}$$

where Q(m,n) is the discrete version of the optical reconstructed wavefront on the object surface, Im and Re are the imaginary and real part of the reconstructed

https://doi.org/10.1017/S0967199413000026 Published online by Cambridge University Press

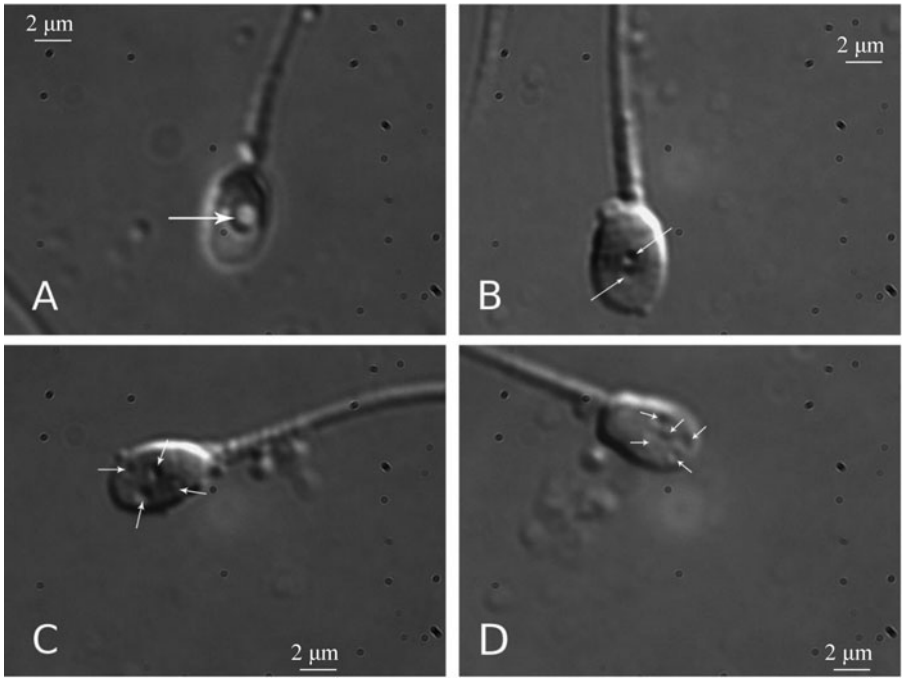


Figure 2 High-power light microscope micrograph of sperm heads (×1500). (*A*) Crater-like appearance of nuclear vacuoles (arrow). (*B–D*) Spermatozoa with one or more vacuoles (arrows).

optical field, respectively. The relationship between the OPD and the thickness of the cell is OPD(m,n) = s(m,n)·(nc – ns), where nc is the refractive index of the cell and ns is the refractive index of the surrounding medium.

Finally, the possibility offered by digital holography to manage the phase of the reconstructed image allows the removal and/or compensation of any unwanted wavefront variations, such as optical aberrations (spherical, coma, tilt) and slide deformations (Ferraro *et al.*, 2003).

Statistical analysis

Statistical analyses were carried out by Student's *t*-test. Probability values lower than or equal to 0.05 were considered to be significant.

Results

In total, 2000 digitalized sperm heads were analysed for six primary parameters (length, width, perimeter, area, number and size of vacuoles). DESA analysis revealed that the mean values for length, width, perimeter and area of the sperm head were 5.18 ± 0.64 µm (mean ± standard deviation (SD)) (range: 3.63–7.87), 3.53 ± 0.45 µm (range: 2.37–5.62), 13.75 ± 1.35 µm (range: 9.64–19.68), 14.12 ± 3.03 µm^2 (range: 7.77–25.82). In the 15 ejaculates, 62.8% of spermatozoa with one or more vacuoles were found. The number of vacuoles per sperm ranged from 0–8 (mean: 2.01 ± 1.78) measuring 0.03–5.90 µm^2 in area (Fig. 2).

We used DHM to evaluate the morphology of 200 of the aforementioned spermatozoa (Fig. 3). Figure 3*A* is an example of an acquired hologram, with the fringe pattern highlighted in the inset. In Fig. 3*B* a pseudocolour plot of the phase-contrast map reconstruction of a human spermatozoon is shown. The colour bar shows the value in rad of the phase difference, which depends on the optical density and thickness of the biological sample. Figure 3*C* illustrates the quantitative reconstructed morphology obtained by applying Equation 3 to the phase-map contrast.

It is important to note that this 3-D image is obtained from the reconstruction of a single acquired hologram, without the use of any mechanical scanning, allowing us to carry out numerical analyses of the six primary sperm parameters mentioned above. No significant differences were observed in the gross morphometric values of the sperm cells analysed (using DESA or DHM; Table 1).

In Fig. 4*A* and Fig. 4*B* we show the quantitative profiles of a spermatozoon along the lines AA′ and BB′ illustrated in Fig. 3*A*, respectively. These profiles show, point by point, a quantitative value of the phase shift due to spermatozoan structure. Quantitative phase shift information from DHM allows us to calculate the volume/mass of the sperm head. In Fig. 5, for example, an isoline plot relative to different heights

https://doi.org/10.1017/S0967199413000026 Published online by Cambridge University Press

Table 1 Mean morphometric values of normal sperm heads obtained by DESA and DHM techniques

Technique	Length (μm ± SD)	Width (μm ± SD)	Perimeter (μm ± SD)	Area (μm2 ± SD)	Volume (μm3 ± SD)
DESA	5.18 ± 0.64	3.53 ± 0.45	13.75 ± 1.35	14.12 ± 1.95	–
DHM	5.62 ± 0.31	2.95 ± 0.51	14.33 ± 1.22	12.98 ± 1.25	8.03 ± 0.75

Mean ± standard deviation (SD) is presented. Significance is calculated with Student's *t*-test. *P*-values <0.05 are considered significant. DESA, digitally enhanced Nomarski microscopy; DHM, digital holographic microscopy.

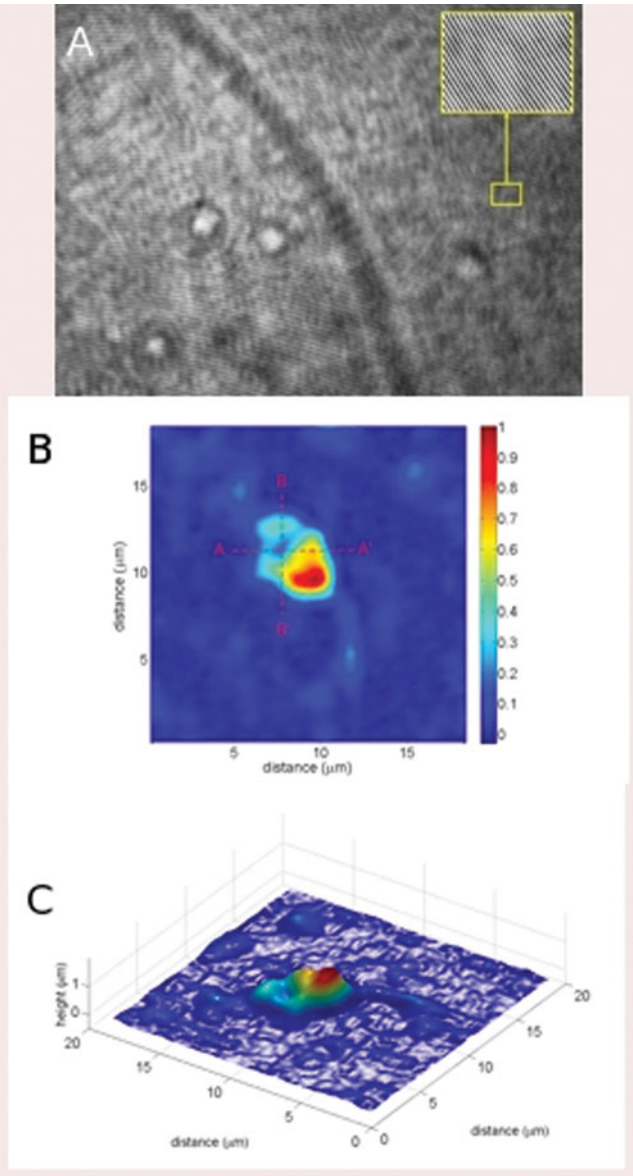


Figure 3 (*A*) Acquired hologram, a region is enhanced in order to show the interference pattern (inset). (*B*) Pseudocolour plot of a phase-contrast map for a human spermatozoon. (*C*) Pseudo three-dimensional (3-D) representation of a human spermatozoon image reconstructed by digital holographic microscopy (DHM).

of the sample is displayed. For each region defined by the isolines, the occupied area and the relative volume has been estimated numerically. The analysis revealed that the mean value for volume in normal sperm is $8.03 \pm 0.72\ \mu m^3$.

In Fig. 6 we show a quantitative comparison between a control spermatozoon and a spermatozoon with vacuoles. Figure 6*A*,*B* illustrates the height profile along the major axis of the sperm head for the defect-free spermatozoon and the spermatozoon with vacuoles, respectively. In Fig. 6*E* the two profiles are shown together to stress the differences. It is worth note that both the shapes and the point-by-point value of the height are different. In particular, the spermatozoon with vacuoles has a distinct depression in the profile (see the arrow in the figure). The profile of the normal spermatozoon is higher than that of the spermatozoon with vacuoles, whereas their 2-D dimensions (such as area, and axes length) are similar. The difference in height difference implies a volume difference between the normal spermatozoon and the spermatozoon with vacuoles.

Table 2 shows three distinct groups of spermatozoa defined using two morphometric variables, head length and head width. The mean values of the volume for the three subpopulations were $5.76 \pm 0.73\ \mu m^3$ (for length $< 2.9\ \mu m$ and width $< 4.2\ \mu m$), $8.24 \pm 0.78\ \mu m^3$ (for $2.9 <$ length $< 3.7\ \mu m$ and $4.2 <$ width $< 5.3\ \mu m$), $10.13 \pm 0.81\ \mu m^3$ (for length $> 3.7\ \mu m$ and width $> 5.3\ \mu m$). Mean values of the total volume of the spermatozoa minus the vacuoles volume are also reported.

Discussion

Here we have used digital holographic microscopy as a novel approach for a more advanced morphological analysis of human spermatozoa, in particular to measure the head volume in the presence and absence of vacuoles.

In human sperm, the presence of vacuoles has been related to poor outcome in ART (Berkovitz *et al.*, 2006), an increase in DNA fragmentation (Franco *et al.*,

https://doi.org/10.1017/S0967199413000026 Published online by Cambridge University Press

Table 2 Mean volumetric values of vacuolated sperm clustered in three different subpopulations

	Volume ($\mu m^3 \pm SD$)	
Sperm dimensions	Total	Total – Vacuoles
Length < 2.9 μm; Width < 4.2 μm	5.76 ± 0.73	3.99 ± 0.76
2.9 < Length < 3.7 μm; 4.2 < Width < 5.3 μm	8.24 ± 0.78	6.40 ± 0.80
Length > 3.7 μm; Width > 5.3 μm	10.13 ± 0.81	8.42 ± 0.79

SD, standard deviation.

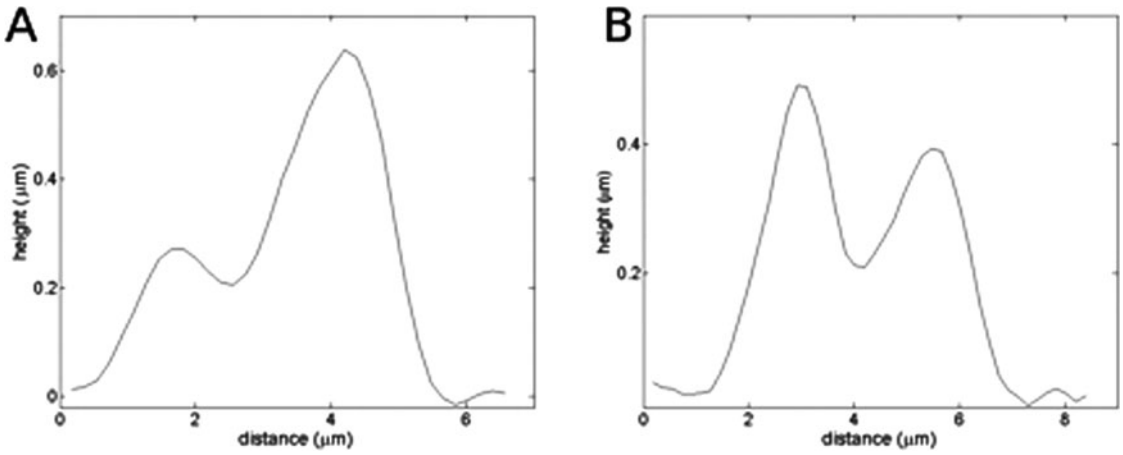


Figure 4 Profile plot along the lines (*A*) AA′ and (*B*) BB′, reported in Fig. 3*B*.

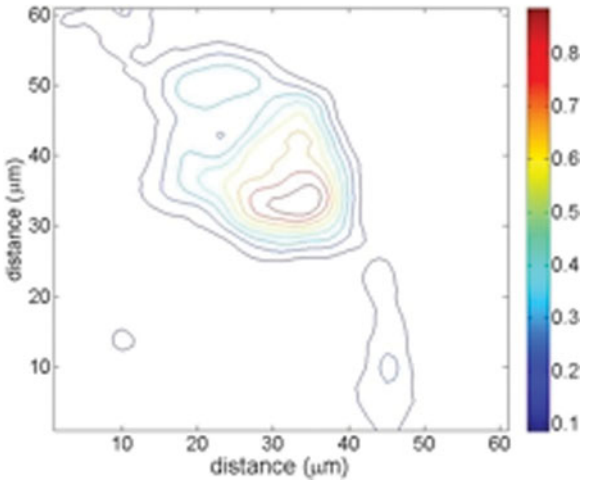


Figure 5 Isolines plot of the reconstructed spermatozoon image.

2008; Wilding *et al.*, 2011) and abnormal chromatin packaging (Franco *et al.*, 2012).

Nuclear vacuoles have been described as a crater defect in the spermatozoa of stallion (Johnson & Hurtgen, 1985), as a pouch formation (Bane & Nicander, 1965), a diadem defect (Blom, 1977) or a nuclear sperm defect (Miller *et al.*, 1982) in bull spermatozoa, and as a crater defect (Johnson & Truitt-Gibert, 1982) or a pouch formation (Bane & Nicander, 1965) in boar spermatozoa. The defect is believed to originate during spermiogenesis, as vacuoles have been found in both early and late spermatids (Johnson & Truitt-Gibert, 1982). Nuclear vacuoles were shown by electron microscopy to be narrow-mouthed invaginations of the nuclear membrane into the nucleoplasm often filled with an amorphous, cytoplasmic material (Barth & Oko, 1989). The predominant locations of the vacuoles are the apical region and the acrosome-postacrosomal sheath junction, but they have also been found throughout the sperm head (Barth & Oko, 1989).

Our results show that spermatozoa with vacuoles had a reduced volume probably due to variation of the inner structure of the sperm head with loss of material. We suggest that vacuolated spermatozoa with normal length and width (Bartoov *et al.*, 2002) should be avoided for selection during the ICSI or IMSI procedure, until we acquire more data on the integrity and volume normal viable spermatozoon.

Recently, we have employed a microfluidic system with DHM on unstained bovine spermatozoa in their natural physiological surroundings (Di Caprio *et al.*, 2010). This situation raises the possibility to use the same technique for a more complete analysis of human

https://doi.org/10.1017/S0967199413000026 Published online by Cambridge University Press

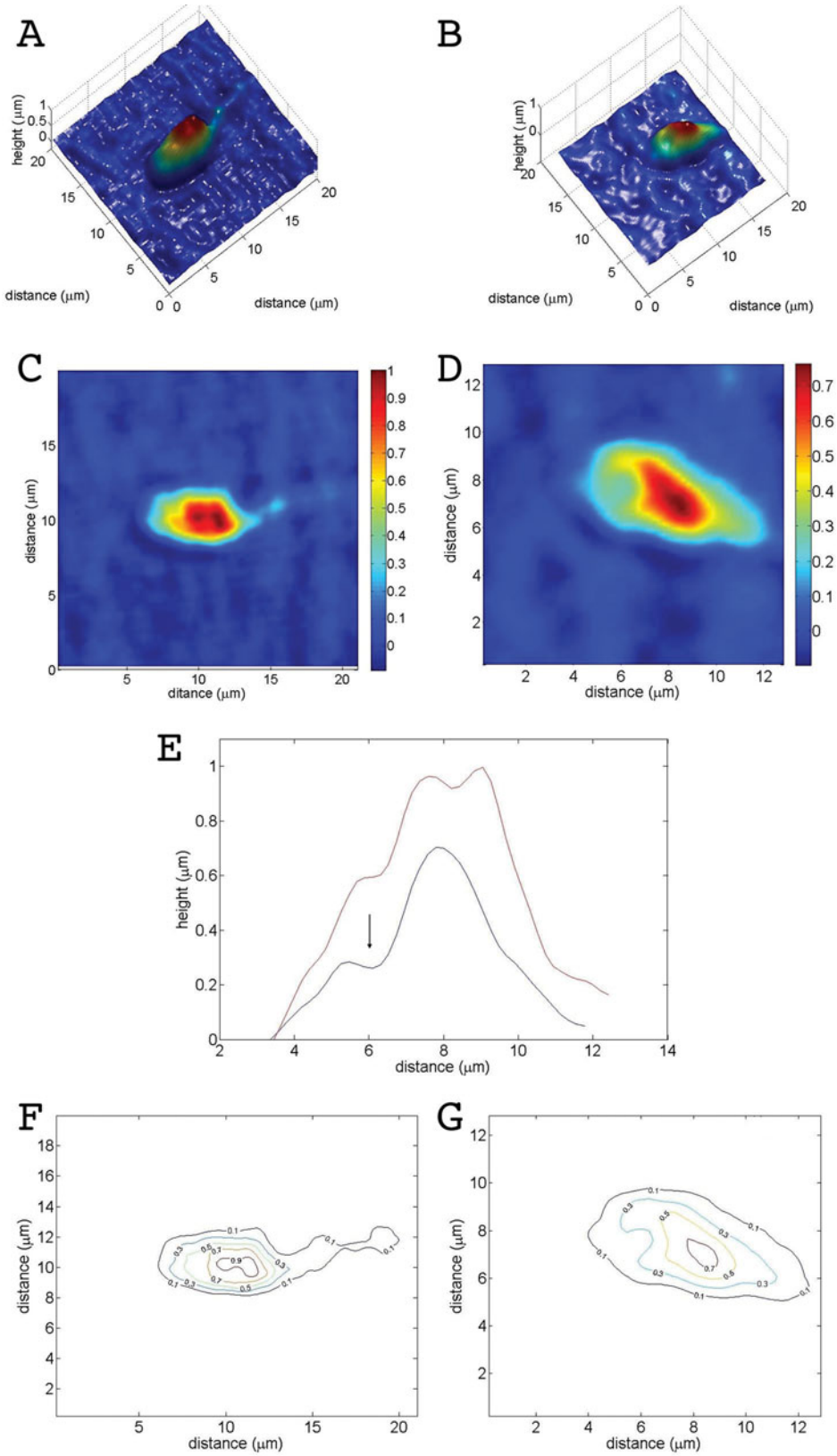


Figure 6 Comparison between a defect-free spermatozoon (left column) and a spermatozoon with vacuoles (right column). Results for a defect-free spermatozoon are reported as a quantitative three-dimensional representation (A), phase-contrast map (C), or as an isolines plot (F). For a spermatozoon with vacuoles, defects are reported as a quantitative three-dimensional representation (B), phase-contrast map (D), or as an isolines plot (G). (E) Comparison between the profile of the spermatozoon with vacuoles (curve indicated by arrow) and one without defects.

https://doi.org/10.1017/S0967199413000026 Published online by Cambridge University Press

spermatozoa, with the additional possibility of sorting cells according to specific morphological criteria.

References

Akaki, M., Nagayasu, E., Nakano, Y. & Aikawa, M. (2002). Surface charge of *Plasmodium falciparum* merozoites as revealed by atomic force microscopy with surface potential spectroscopy. *Parasitol. Res.* **88**, 16–20.

Bane, A. & Nicander, L. (1965). Pouch formations by invaginations of the nuclear envelope of bovine and porcine sperm as e sign of disturbed spermiogenesis. *Nord Vet. Med.* **17**, 628–32.

Barth, A.D. & Oko, R.J. (1989). *Abnormal Morphology of Bovine Spermatozoa*, Ames, Iowa, USA: Iowa State University Press.

Bartoov, B., Eltes, F., Pansky, M., Lederman, H., Caspi, E. & Soffer, Y. (1999). Estimating fertility potential via semen analysis data. *Hum. Reprod.* **8**, 65–70.

Bartoov, B., Berkovitz, A., Eltes, F., Kogosowski, A., Menezo, Y. & Barak, Y. (2002). Real-time fine morphology of motile human sperm cells is associated with IVF–ICSI outcome. *J. Androl.* **23**, 1–8.

Berkovitz, A., Eltes, F., Soffer, Y., Zabludovsky, N., Beyth, Y., Farhi, J., Levran, D. & Bartoov, B. (1999). ART success and *in vivo* sperm cell selection depend on the ultramorphological status of spermatozoa. *Andrologia* **31**, 1–8.

Berkovitz, A., Eltes, F., Lederman, H., Peer, S., Ellenbogen, A., Feldberg, B. & Bartoov, B. (2006). How to improve IVF-ICSI outcome by sperm selection. *Reprod. Biomed. Online* **12**, 634–8.

Blom, E. (1977). Sperm morphology with reference to bull infertility. In *Proc. First All-India Symp. Anim. Reprod., Ludhiana* (ed. E. Blom) pp. 61–81.

Bon, P., Maucort, G., Wattellier, B. & Monneret, S. (2009). Quadriwave lateral shearing interferometry for quantitative phase microscopy of living cells. *Opt. Express* **17**, 13080–94.

Carl, D., Kemper, B., Wernicke, G. & von Bally, G. (2004). Parameter optimized digital holographic microscope for high-resolution living cell analysis. *Appl. Opt.* **43**, 6536–44.

Charrière, F., Marian, A., Montfort, F., Kuehn, J., Colomb, T., Cuche, E., Marquet, P. & Depeursinge, C. (2006). Cell refractive index tomography by digital holographic microscopy. *Opt. Lett.* **31**, 178–80.

Coppola, G., Ferraro, P., Iodice, M., De Nicola, S., Finizio, A. & Grilli, S. (2004). Digital holographic microscope for static and dynamic characterization of MEMS. *Meas. Sci. Technol.* **1**, 529–39.

Crha, I., Zakova, J., Huser, M., Ventruba, P., Lousova, E. & Pohanka, M. (2011). Digital holographic microscopy in human sperm imaging. *J. Assist. Reprod. Genet.* **28**, 725–9.

Cuche, E., Marquet, P. & Depeursinge, C. (1999). Simultaneous amplitude-contrast and quantitative phase-contrast microscopy by numerical reconstruction of Fresnel off-axis holograms. *Appl. Opt.* **38**, 6994–7001.

Dadoune, J.P. (2003). Expression of mammalian spermatozoal nucleoproteins. *Microsc. Res. Tech.* **61**, 56–75.

Di Caprio, G., Gioffre`, M.A., Saffioti, N.A., Grilli, S.A., Ferraro, P.A., Puglisi, R.A., Balduzzi, D.A., Galli, A.A. & Coppola, G. (2010). Quantitative label-free animal sperm imaging by means of digital holographic microscopy. *IEEE J. Sel. Top. Quant. Electron.* **16**, 833–40.

Dubois, F., Joannes, L. & Legros, J.C. (1999). Improved three-dimensional imaging with a digital holographic microscope with a source of partial spatial coherence. *Appl. Opt.* **38**, 7085–94.

Elder, K. & Dale, B. (2011). *In-vitro Fertilization*, 3rd edn, Cambridge, UK: Cambridge University Press, 35 pp.

Ferraro, P., De Nicola, S., Finizio, A., Coppola, G., Grilli, S., Magro, C. & Pierattini, G. (2003). Compensation of the inherent wave front curvature in digital holographic coherent microscopy for quantitative phase-contrast imaging. *Appl. Opt.* **42**, 1938–46.

Ferraro, P., Coppola, G., Alfieri, D., De Nicola, S., Finizio, A. & Pierattini, G. (2004). Controlling images parameters in the reconstruction process of digital holograms. *IEEE JSTQE* **10**, 829–83.

Ferraro, P., Grilli, S., Alfieri, D., De Nicola, S., Finizio, A., Pierattini, G., Javidi, B., Coppola, G. & Striano, V. (2005). Extended focused image in microscopy by digital holography. *Opt. Express* **13**, 6738–49.

Franco Jr., J.G., Baruffi, R.L., Mauri, A.L., Petersen, C.G., Oliveira, J.B. & Vagnini, L. (2008). Significance of large nuclear vacuoles in human spermatozoa: implications for ICSI. *Reprod. Biomed. Online* **17**, 42–5.

Franco Jr., J.G., Mauri, A.L., Petersen, C.G., Massaro, F.C., Silva, L.F., Felipe, V., Cavagna, M., Pontes, A., Baruffi, R.L., Oliveira, J.B. & Vagnini, L.D. (2012). Large nuclear vacuoles are indicative of abnormal chromatin packaging in human spermatozoa. *Int. J. Androl.* **35**, 46–51.

Gerton, G. (2002). Function of the sperm acrosome. In *Fertilization* (ed. D. Hardy), pp. 265–302, San Diego: Academic Press.

Johnson, L.A. & Truitt-Gibert, A.J. (1982). Incidence and ultrastructure of abnormalities in porcine spermatozoa. *Ann. N.Y. Acad. Sci.* **383**, 466–8.

Johnson, L.A. & Hurtgen, J.P. (1985). The morphological and ultrastructural appearance of the crater defect in stallion spermatozoa. *Gamete Res.* **12**, 41–6.

Kemper, B.D., Carl Schnekenburger, J., Bredebusch, I., Schäfer, M., Domschke, W. & von Bally, G. (2006). Investigation on living pancreas tumor cells by digital holographic microscopy. *J. Biomed. Opt.* **11**, 34005.

Kou, S.S., Waller, L., Barbastathis, G. & Sheppard, C.J.R. (2010). Transport-of-intensity approach to differential interference contrast (TI-DIC) microscopy for quantitative phase imaging. *Opt. Lett.* **35**, 447–9.

Kruger, T.F., Acosta, A.A., Simmons, K.F., Swanson, R.J., Matta, J.F. & Oehninger, S. (1988). Predictive value of abnormal sperm morphology *in vitro* fertilization. *Fertil. Steril.* **49**, 112–7.

Marquet, P., Rappaz, B., Magistretti, P.J., Cuche, E., Emery, Y., Colomb, T. & Depeursinge, C. (2005). Digital holographic microscopy: a non invasive contrast imaging technique allowing quantitative visualization of living cells with sub wavelength accuracy. *Opt. Lett.* **30**, 468–70.

Mashiach, R., Fisch, B., Eltes, F., Tadir, Y., Ovadia, J. & Bartoov, B. (1992). The relationship between sperm ultrastructural features and fertilizing capacity *in vitro*. *Fertil. Steril.* **57**, 1052–7.

https://doi.org/10.1017/S0967199413000026 Published online by Cambridge University Press

Miller, D.M., Hrudka, F., Cates, W.F. & Mapletoft, R.J. (1982). Infertility in a bull with a nuclear sperm defect: a case report. *Theriogenology* **17**, 611–21.

Oko, R.J. (1995). Developmental expression and possible role of perinuclear theca proteins in mammalian spermatozoa. *Reprod. Fertil. Dev.* **7**, 777–97.

Palermo, G., Joris, H., Devroey, P. & Van Steirteghem, A.C. (1992). Pregnancies after intracytoplasmic injection of single spermatozoon into an oocyte. *Lancet* **340**, 17–8.

Rothery, AM., Gorelik, J., Bruckbauer, A., Yu, W., Korchev, Y.E. & Klenerman, D. (2003). A novel light source for SICM–SNOM of living cells. *J. Microsc.* **209**, 94–101.

Steptoe, P.C. & Edwards, R.G. (1978). Birth after the reimplantation of a human embryo. *Lancet* **12**, 366.

Wilding, M., Coppola, G., Di Matteo, L., Palagiano, A., Fusco, E. & Dale, B. (2011). Intracytoplasmic injection of morphologically selected spermatozoa (IMSI) improves outcome after assisted reproduction by deselecting physiologically poor quality spermatozoa. *J. Assist. Reprod. Genet.* **28**, 253–62.

Yoshinaga, K. & Toshimori, K. (2003). Organization and modifications of sperm acrosomal molecules during spermatogenesis and epididymal maturation. *Microsc. Res. Tech.* **61**, 39–45.

https://doi.org/10.1017/S0967199413000026 Published online by Cambridge University Press